Energetics of Cu adsorption and intercalation at graphite step edges

Yong Han, Ann Lii-Rosales, Michael C. Tringides, James W. Evans, and Patricia A. Thiel

Phys. Rev. B **99**, 115415 — Published 11 March 2019

DOI: 10.1103/PhysRevB.99.115415

Energetics of Cu adsorption and intercalation at graphite step edges

Yong Han,[1,2] Ann Lii-Rosales,[1,3] Michael C. Tringides,[1,2] James W. Evans,[1,2] and Patricia A. Thiel[1,3,4]

[1]*Ames Laboratory, U. S. Department of Energy, IA 50011, United States*
[2]*Department of Physics and Astronomy, Iowa State University, Ames, IA 50011, United States*
[3]*Department of Chemistry, Iowa State University, Ames, IA 50011, United States*
[4]*Department of Materials Science and Engineering, Iowa State University, Ames, IA 50011, United States*

Abstract

To assess the energetics of Cu intercalation on defective graphite, the chemical potentials and binding energies for Cu at graphite step edges are calculated for three main configurations: an isolated atom; a chain; and an atom attached to a chain. As expected, for Cu interacting directly with a graphite step edge, the strength of interaction depends on the stability of the step, with Cu binding more strongly at a less-stable step. However, the relationship is reversed when considering binding of a Cu atom attached to a chain. Taken together, these trends mean that if the graphite step is less stable, as for the zigzag step, then decorating the step with a Cu chain facilitates intercalation by additional Cu atoms (which are less strongly bound to the decorated step). For more stable steps, intercalation is optimal without decoration. We also calculate the diffusion barrier for atomic Cu on top of the graphite terrace, and in the uppermost gallery, finding values of 0.008 eV and 0.021 eV, respectively. These values are very small, indicating that the minimum barrier for a Cu atom to detach from a step and move to a terrace or gallery is dominated by the difference in binding energies. For intercalation, this minimum barrier is 1.4 to 3.1 eV and depends strongly on step configuration.

I. INTRODUCTION

Layered materials, also called van der Waals materials, have long been known as versatile and tunable materials, because they readily accept diverse foreign materials into the galleries (the spaces between layers) [1]. This is known as intercalation. Recently there has been an explosion of interest in two-dimensional (2D) materials. The 2D materials consist of single or few layers derived from a parent layered compound, e.g. graphene usually supported on a solid substrate, as well as vertically stacked heterostructures derived from layered materials. The 2D materials also offer the opportunity to tune properties via intercalation, and such opportunity has been, and continues to be, heavily explored [2, 3, 4, 5, 6, 7]. Intercalation can also be used as a means to promote exfoliation of layered materials or to decouple an as-grown layer from the substrate, hence facilitating production of 2D materials [8, 9, 10, 11, 12, 13, 14]. The most heavily-investigated system in this regard is supported graphene [6, 5, 4, 2]. However, the mechanism by which the intercalant moves from the surface to the galleries has been somewhat elusive. Proposed mechanisms include penetration through vacancy defects in graphene in certain systems [15, 16, 17].

Graphite is the prototypical layered material, and we have recently undertaken an investigation into the possibility of surface intercalation by elemental transition metals and rare earth metals on graphite in ultrahigh vacuum [18, 19, 20, 21]. We have found that encapsulated metal islands can form if defects are introduced deliberately, prior to metal deposition, via ion bombardment of graphite. It is also necessary to hold the sample at elevated temperature during metal deposition. We postulated that the defects serve as entry portals for metal atoms, while the elevated temperatures inhibit formation of metal clusters adsorbed on top of the surface and keep the portals open. This study will focus on the Cu-graphite system. A schematic of a Cu atom passing from a terrace, over the edge of a vacancy defect (or step), and into a gallery, is shown in Fig. 1. For Cu, the encapsulated Cu islands are particularly large — as tall as 40 nm and as wide as 600 nm [19]. The ability to form large Cu islands in this system suggests a path to micropatterning electrical contacts or heat sinks, in electrical circuits that utilize graphene. With regard to other applications of Cu-carbon systems, recent experimental finding of the Cu-carbon composite as a high-performance electrical conductor to induce the world highest current density [22], the stability of which depends on Cu atom diffusion energetics.

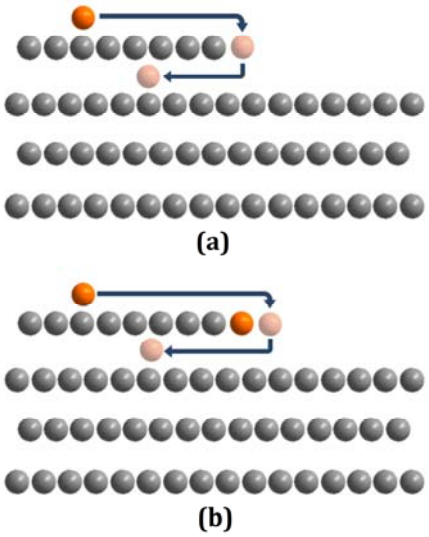

FIG. 1. Schematic (side view) of a Cu atom passing from the top of a graphite terrace, past the edge of a vacancy defect or step, into the topmost gallery of graphite. Gray balls represent C atoms, and orange balls represent Cu atoms. For the Cu atoms, the dark shade represents an initial position and light shades represent subsequent positions as the top Cu atom moves into the gallery. (a) The edge is clean. (b) The edge is pre-decorated with Cu atoms.

In the model above, operation and structure of the entry portals is very important, but only limited information exists about them at this time. It is likely that a wide variety of defects are introduced by ion bombardment, from structural vacancies to interstitial carbon atoms [23, 24]. Our experiments consistently show that the number density of

intercalated metal islands is much lower than the density of defects in the graphite surface [20, 19]. A reasonable explanation is that an effective portal (vacancy) has a minimum size corresponding to more than one missing C atom, and only a small fraction of defects meets this requirement. Previously, Büttner *et al*. studied Cs intercalation at a defect-rich graphite surface. Their density-functional-theory (DFT) calculations showed that more than 4 neighboring C atoms in a graphene sheet must be missing, in order to obtain a reasonably low activation barrier for passage of the large Cs through the defect [25]. More recently, Yu et al. reported that the barrier for a Dy atom to pass through a graphene vacancy decreases with increasing number of missing C atoms, m, falling sharply from 2 eV at m = 2, to 0.3 eV at m = 3 [26].

Focusing on the size of the portal may, however, be an oversimplification. The effectiveness of a portal for intercalation could depend not only on its size, but on the arrangement of C atoms around its perimeter. The most stable C atom configurations at graphene vacancies can usually be described as mixtures of 5- and 6-membered C rings surrounding a larger hole. Sometimes the perimeter of the hole also contains coordinatively-unsaturated C atoms (cus-C atoms), i.e. C atoms bonded to fewer than 3 nearest neighbors in the graphene sheet [27, 28, 29, 30, 31, 32]. Examples are shown in Fig. 2. A second important question is whether a portal is more effective for intercalation when it is entirely clean (Fig. 1(a)), or when its edges are pre-decorated with metal atoms (Fig. 1(b)). One could imagine that metal bonding to the free C edge is stronger than metal-metal bonding, so decoration would effectively passivate the step and facilitate passage of other metal atoms over the vacancy edge. However, if edge passivation with metal atoms is necessary, then the minimum size for an active portal could be very large, requiring several missing C atoms. A simple geometric estimate indicates that $m > 6$ would be necessary to accommodate two coplanar Cu atoms, for instance.

In principle, one can use DFT to simulate the intercalation of Cu atoms via a portal with various structures, but the computational expense will be substantial due to the variety of the portal structures and the necessarily-large lateral supercell sizes. However, irrespective of the size of the active portals, their edges might be regarded as composed of portions of step edges of different orientations and terminations. Thus, the purpose of this paper is to take a first step to address intercalation at portals, by examining the energetics of Cu atoms at and near extended graphite step edges with different atomic configurations. The graphite step edges, which are based upon known configurations at the edges of graphene sheets, contain the same elements as vacancy perimeters: 5-, 6-, and (additionally) 7-atom C rings, and cus-C atoms. This approach yields insights into the way in which Cu adsorption and intercalation depend on the atomic arrangement of C atoms at a graphite step or portal, and on whether that step or portal is decorated with Cu.

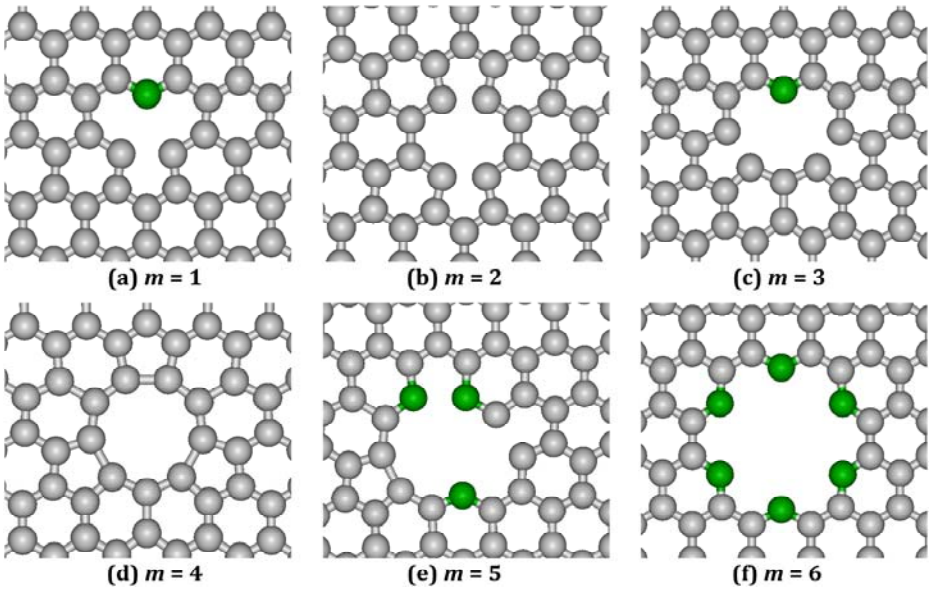

FIG. 2. Structures (top views) of graphene vacancies optimized from our DFT calculations. The number of missing carbon atoms is *m*. Gray balls are C atoms bonded to 3 others; green balls are C atoms bonded to only 2, i.e. cus-C atoms. (a) *m* = 1, (b) *m* = 2. (c) *m* = 3, (d) *m* = 4, (e) *m* = 5, and (f) *m* = 6. These structures are supported by previous calculations [27, 28, 29] and, in some cases, by transmission-electron-microscopy (TEM) observations [30, 31]. For a given *m*, more than one configuration is possible [28, 29, 32]. Here we only show the arrangement with the largest central hole for each *m*. The green balls represent cus-C atoms.

In this paper, we perform first-principles DFT total-energy calculations for the graphene, graphite, Cu-graphene, and Cu-graphite systems using the Vienna *Ab Initio* Simulation Package (VASP) code [33]. The projector-augmented-wave (PAW) method [34] is used for the electron-core interactions. The pseudopotentials were generated and released in 2013 by the VASP group. For all Cu-C systems, we use the optB88-vdW functional, where the exchange functional is optimized for the correlation part [35], to approximately account for dispersion interactions. Spin-polarization effects and dipole corrections have been taken into account in all DFT calculations. The Γ-centered ***k*** mesh will be specified depending on the system to be calculated. The vacuum thickness between two adjacent slab replicas is not less than 1.6 nm. The force-convergence criterion is 0.1 eV/nm. We perform benchmarking calculations for bulk properties of graphite and Cu, as well as the graphene vacancy formation energies (see Appendix A) to confirm the validity of the DFT method.

This paper is arranged as follows. Section II briefly presents results for the energies of clean or undecorated graphite steps with different atomic configurations and compares them with clean graphene edges. Section III focuses on Cu binding at graphite step edges, and Section IV describes the energetics of Cu intercalation at different step edges. Since Cu atom diffusion can contribute to the barrier for intercalation, this section also presents

calculations of Cu atom diffusion barriers. Section V provides further discussion, and we draw conclusions in Section VI.

II. RESULTS FOR CLEAN GML AND GRAPHITE STEPS

We first briefly describe results and analysis for energies of clean or undecorated steps on graphite, together with similar results for graphene, which will be relevant for our analysis of Cu binding at step edges. In the absence of reconstruction, the close-packed steps on graphite surfaces, or the edges of a freestanding GML, can have either zigzag (zz) or armchair (ac) configurations, as shown in Fig. 3. The steps consist entirely of non-sp^2 C atoms. For a freestanding GML, reconstructions of the edges were predicted by Koskinen *et al*. from DFT [36] and confirmed by experiments [37]. These reconstructions involve transition from purely 6-membered rings to a combination of 5-, 6-, or 7-membered rings at the edge. In order to generate a self-consistent set of step energies as a basis for further calculations, we recalculate the edge energies for 4 types of GML edges (see Fig. 3): zz, ac677 (where the numbers denote the ring sequence at a reconstructed edge), ac, and zz57. Further, we replace ac56 in Ref. [36] with a new type of reconstructed armchair edge ac5666 (see Fig. 3 again) because ac56 has a much higher edge energy than the other 4 types [36] and is not evident in experiments, while an ac566 segment has been observed in experiment [37].

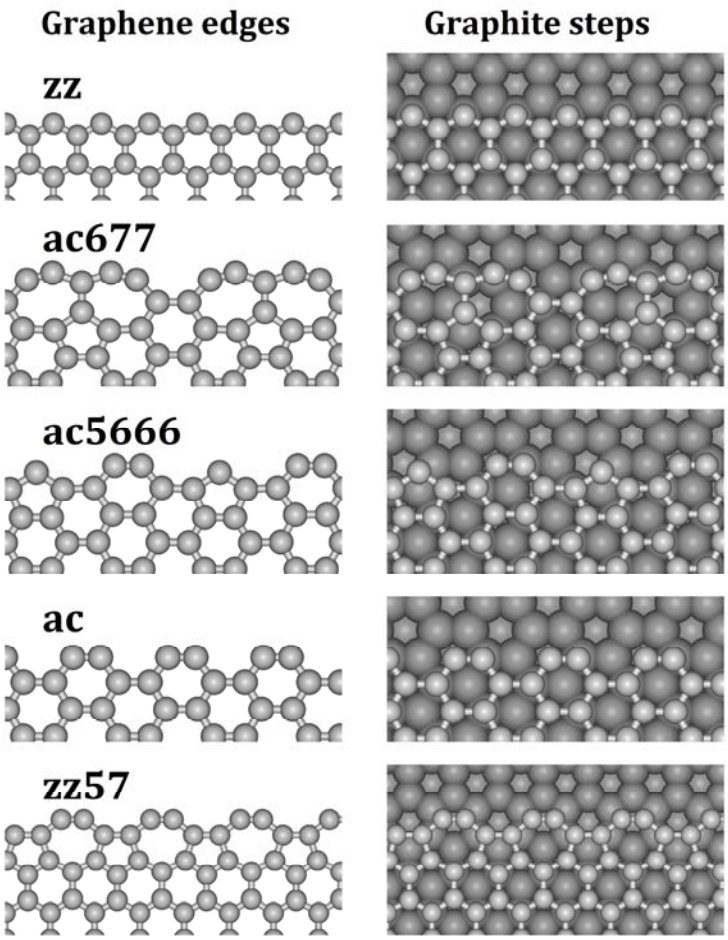

FIG. 3. The geometries of graphene edges (left) and graphite step edges (right) optimized from our optB88-vdW calculations: zz (zigzag), ac677 (reconstructed armchair), ac5666 (reconstructed armchair), ac (armchair), and zz57 (reconstructed zigzag) from top to bottom. The order of the geometries from bottom to top corresponds to the order of their edge energies from lowest to highest.

The GML edge energy can be calculated as

$$\varepsilon_{\text{edge}} = \frac{E_{\text{ribbon}} - N_{\text{ribbon}}\sigma_{\text{GML}}}{2l}, \quad (1)$$

where E_{ribbon} is the total energy of the graphene ribbon with two symmetric edges in a supercell, N_{ribbon} is the total number of C atoms in the ribbon, l is the length of the edge, and σ_{GML} is the energy per C atom in a freestanding perfect GML without edges. By this definition, lower step energy corresponds to a more stable step. For graphite step edges, we construct a geometry using 3 complete GMLs (the bottommost GML is fixed) to represent the graphite substrate supporting the GML ribbon, and the step edge energy can be still calculated from Eq. (1), but $E_{\text{ribbon}} = E_{\text{rs}} - E_{\text{substrate}}$, where E_{rs} is the total energy of the graphene ribbon plus the substrate, and $E_{\text{substrate}}$ is the energy of the substrate,

while σ_{GML} is the energy per C atom in a complete GML (without steps) supported on the same substrate. For details of the analysis, see Appendix A.

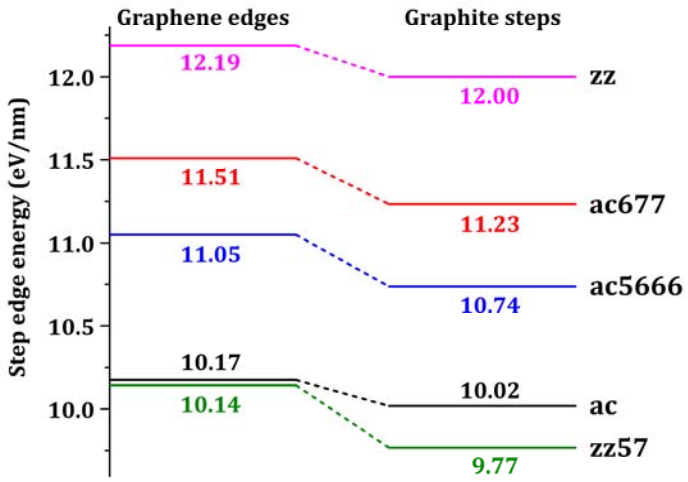

FIG. 4. The edge energy levels of graphene edges and graphite steps corresponding to Fig. 3.

The geometries of 5 types of graphene edges and graphite step edges optimized from our optB88-vdW calculations are shown in Fig. 3, and the corresponding edge energies are plotted in Fig. 4. From Fig. 4, the order of GML edge energy levels of zz, ac677, ac, and zz57 is the same as that in Ref. [36], although there are small differences in magnitude, likely from the use of different functionals. The lowest-energy (most stable) step is zz57, with ac slightly higher, and ac5666 above that. Reconstruction serves to stabilize the zz step and destabilize the ac step. Graphite steps, in comparison to their GML counterparts, have edge energies that are lower by 0.1 to 0.4 eV/nm. The gap between the lowest two (zz57 and ac) is larger for graphite than graphene, where they are nearly degenerate (see Fig. 4). Thus, for both graphene edges and graphite step edges, the energy order of the 5 types of edges is zz57 < ac < ac5666 < ac677 < zz.

Comparison with experiments is limited. For graphene, Koskinen *et al*. [37] have argued convincingly (from TEM data of Girit *et al*. [38]) that zz > zz57 in energy, consistent with the upper and lower bounds in the sequence above. But an analogous measurement for graphite is lacking. On graphite, the most relevant experiments reported to date are STM measurements which show steps with gross orientations falling parallel to those expected for zz or ac. These two orientations are rotated by 30°. However, such measurements have not achieved the atomic-scale resolution necessary to distinguish reconstructed steps from unreconstructed ones [39]. Furthermore, there has been no experimental comparison of stabilities of zz and ac steps, reconstructed or not, for either graphite or graphene.

III. ENERGETICS OF Cu BOUND AT GRAPHITE STEP EDGES

To assess the relative stability of various structures involving Cu binding on graphite, particularly at step edges, it is convenient to define a chemical potential of Cu as [19]

$$\mu_{\mathrm{Cu}} = \frac{E_{\mathrm{tot}} - E_{\mathrm{graphite}}}{n} - E_{\mathrm{Cu}}, \quad (2)$$

where E_{tot} is the total energy of the Cu structure plus graphite system, E_{graphite} is the energy of the relaxed graphite substrate (without Cu) with or without steps, n is the total number of Cu atoms in the supercell, and E_{Cu} is the energy of one Cu atom in the gas phase. This chemical potential accounts for both Cu-Cu and Cu-C interactions for all the Cu in the structure considered. Lower chemical potential corresponds to a configuration with a stronger interaction of a Cu atom with other atoms on average. For one adatom (n = 1) adsorbed on a perfect graphite substrate, μ_{Cu} reduces to the conventional adsorption energy

$$E_{\mathrm{ads}} = E_{\mathrm{tot}} - E_{\mathrm{graphite}} - E_{\mathrm{Cu}}. \quad (3)$$

To provide additional insight into the energy landscape of one specific Cu atom bound to different positions on the graphite terrace, at a step edge (with or without other Cu atoms), and at sites in the gallery beneath the top GML, we also define a binding energy for this Cu as

$$E_{\mathrm{bind}} = E_{\mathrm{tot}} - E_{\mathrm{substrate}} - E_{\mathrm{Cu}}, \quad (4)$$

where $E_{\mathrm{substrate}}$ is the energy of the optimized structure of the substrate, which is a graphite step decorated or not decorated by a Cu chain, as discussed below. For the case where the substrate is not pre-decorated by a Cu chain, i.e., for a pure graphite substrate, Eq. (4) reduces to Eq. (3). Lower E_{bind} indicates stronger binding between the Cu atom and the substrate.

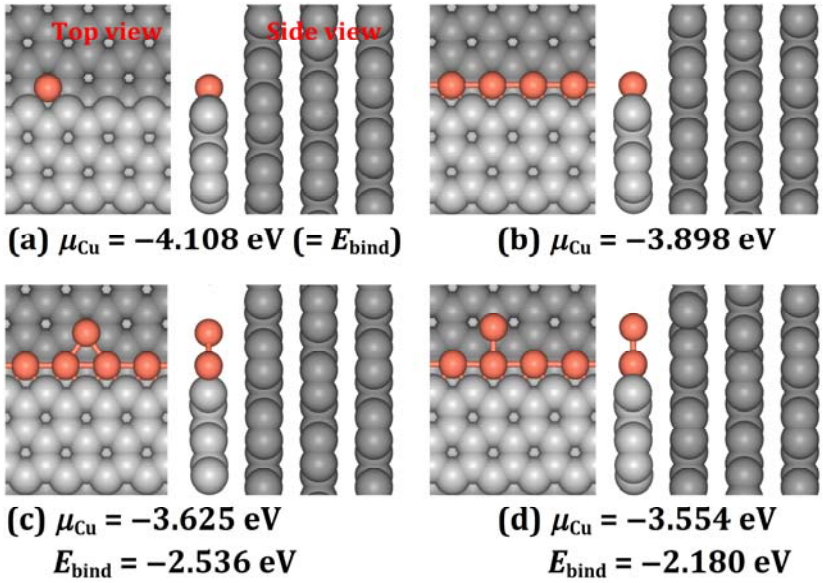

FIG. 5. Top and side views of geometries of Cu atoms (orange colored) bound at zz and Cu-decorated zz step edges optimized from our optB88-vdW calculations. Carbon atoms at the top (bottom) terrace are light (dark) gray balls. Each panel shows one complete supercell. The corresponding DFT energy of each structure is provided. (a) One Cu atom per supercell is bound at the zz step edge (n = 1). (b) A contiguous Cu atom chain is bound at the zz step edge (n = 4). (c) and (d) One Cu atom per supercell is bound at the Cu-chain-decorated zz step edge (n = 5).

Within the framework of these definitions, it is useful to examine the stability of Cu at a graphite step. For this purpose, we examine three step geometries: the least-stable step, zz (Fig. 5); a step with intermediate stability, ac (Fig. 6); and the most stable step, zz57 (Fig. 7). Our analysis uses a lateral supercell with width corresponding to n_{width} = 4 C atoms collinear with the macroscopic direction of the step edge. Consequently, a calculation with a step decorated by a contiguous chain of Cu atoms includes n = 4 Cu atoms. For these geometries, we always use 3 complete GMLs with the bottommost GML frozen to represent the graphite substrate supporting a GML ribbon with two edges. During structure optimization, the top GML ribbon with a finite width (or the top GML of substrate) sometimes can have a lateral shift, which is caused by the finite supercell size. To avoid this artificial effect, when it happens, we fix the lateral coordinates of the C atoms at one edge (as well as below the edge) without adsorbed Cu and let the C atoms be free at another edge with absorbed Cu. Except for the abovementioned frozen or selectively-fixed C atoms, other atoms are fully relaxed. We focus on three types of Cu configurations: a single atom (n = 1, e.g. Fig. 5(a)); an extended Cu chain which saturates the step (n = 4, e.g. Fig. 5(b)); and an extended chain with an extra Cu atom attached (n= 5, e.g. Figs. 5(c) and 5(d)). Here, as above, n denotes the number of Cu atoms in the supercell. In the n = 4 configuration, the Cu atoms form a contiguous chain that is in direct contact with the step, whereas for n = 5, one Cu atom attaches to the Cu chain but not directly to the graphite step. In two cases, there are two forms of a (meta)stable configuration that are close in energy: n = 5 at the zz

step (Figs. 5(c) and 5(d)), and n = 4 at the zz57 step (Figs. 7(c) and 7(d)). In these cases, we focus on the lower-energy form. Trends in chemical potentials are summarized in Fig. 8 and Table I.

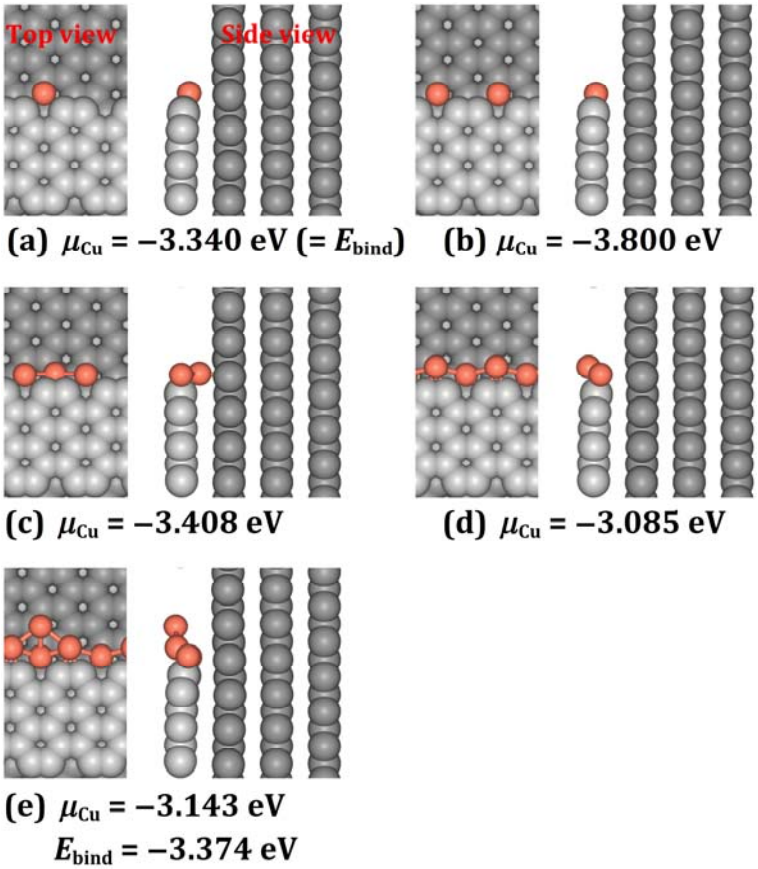

FIG. 6. Top and side views of geometries of Cu atoms (orange colored) bound at ac and Cu-decorated ac step edges optimized from our optB88-vdW calculations. Carbon atoms at the top (bottom) terrace are light (dark) gray balls. Each panel shows one complete supercell. The corresponding DFT energy of each structure is provided. (a) One Cu atom per supercell is bound at the ac step edge (n = 1). (b) Two Cu atoms per supercell are bound at the ac step edge (n = 2). (c) Three Cu atoms per supercell are bound at the zz step edge (n = 3). (d) A contiguous Cu atom chain is bound at the ac step edge (n = 4). (e) One Cu atom per supercell is bound at the Cu-chain-decorated ac step edge (n = 5).

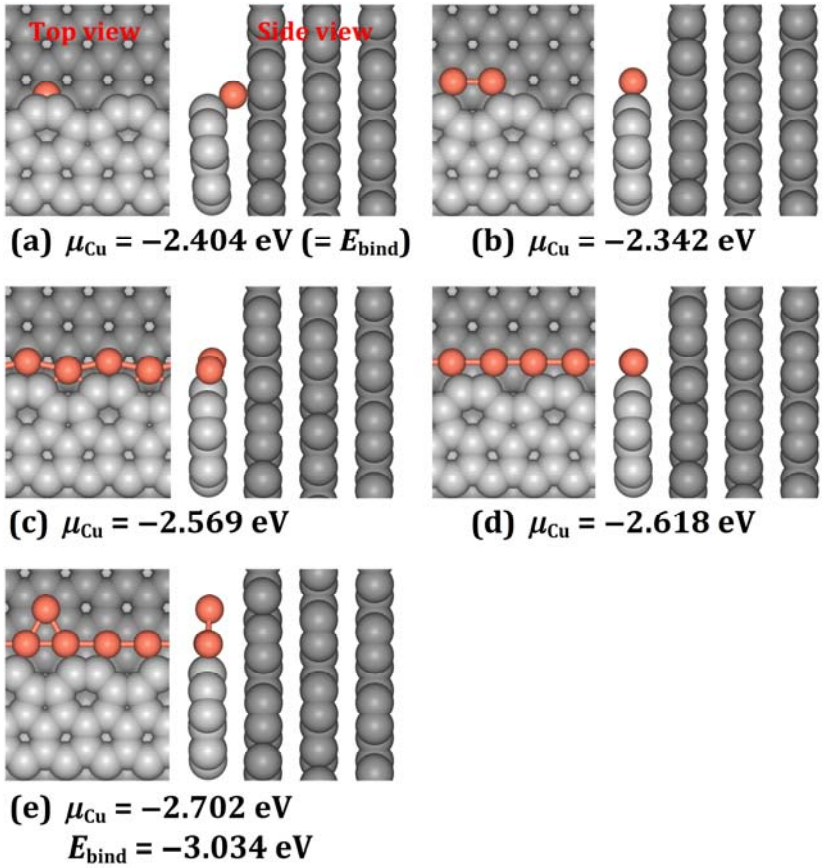

FIG. 7. Top and side views of geometries of Cu atoms (orange colored) bound at zz57 and Cu-decorated zz57 step edges optimized from our optB88-vdW calculations. Carbon atoms in the top (bottom) terrace are light (dark) gray balls. Each panel shows one complete supercell. The corresponding DFT energy of each structure is provided. (a) One Cu atom per supercell is bound at the zz57 step (n = 1). (b) Two Cu atoms per supercell are bound at the zz57 step (n = 2). (c) and (d) A Cu atom chain saturates the zz57 step (n = 4). (e) One Cu atom per supercell is bound to the most stable Cu chain at a zz57 step (n = 5).

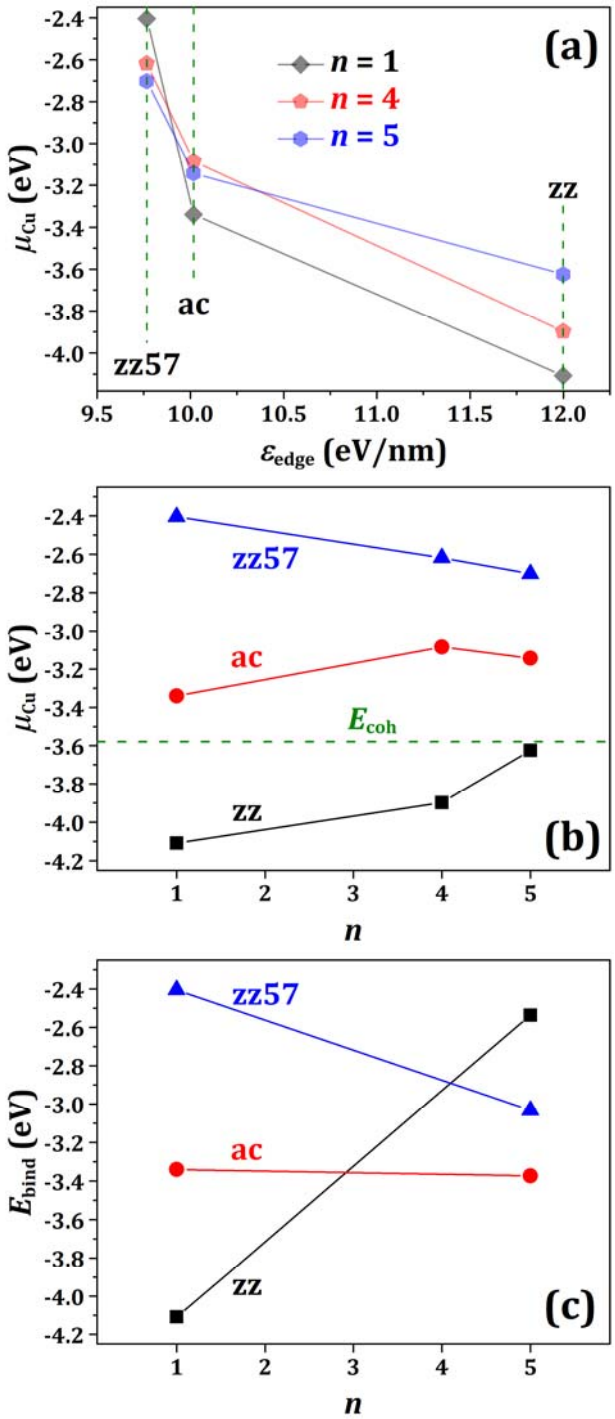

Fig. 8. Trends in chemical potential and binding energies of Cu at graphite step edges, based on DFT results in Figs. 5 to 7. Connecting lines between points are simply drawn to highlight trends. (a) μ_{Cu} as a function of graphite step edge energy ε_{edge}. (b) μ_{Cu} as a function of the number, n, of Cu atoms per supercell. The horizontal dashed line denotes the calculated cohesive energy E_{coh} of bulk Cu (listed in Table II in Appendix A). (c) E_{bind} as a function of n.

Table I. Edge energies ($\varepsilon_{\mathrm{edge}}$) of clean graphite steps corresponding to Figs. 3 and 4; chemical potentials (μ_{Cu}) and binding energies (E_{bind}) of Cu in different configurations at graphite steps corresponding to Figs. 5 to 7.

Step type	n	$\varepsilon_{\mathrm{edge}}$ (eV/nm)	μ_{Cu} (eV)	E_{bind} (eV)
zz	0	12.00		
	1		-4.108	-4.108
	4		-3.898	
	5		-3.625	-2.536
ac	0	10.02		
	1		-3.340	-3.340
	2		-3.800	
	3		-3.408	
	4		-3.085	
	5		-3.143	-3.374
zz57	0	9.77		
	1		-2.404	-2.404
	2		-2.342	
	4		-2.618	
	5		-2.702	-3.034

First, we compare μ_{Cu} values, varying the type of step edge for a given Cu-configuration type n. For a single Cu atom (n = 1) at zz, ac, and zz57 step edges, μ_{Cu} is -4.108, -3.340, and -2.404 eV, respectively. Noting that $\mu_{\mathrm{Cu}} = E_{\mathrm{bind}} = E_{\mathrm{ads}}$ for these 3 cases, the order of the stabilities of 3 types of clean step edges is opposite to the order of the Cu binding (or adsorption) strengths, i.e., the less stable the edge, the stronger the binding of atomic Cu. This trend is shown by the diamonds in Fig. 8(a). The same trend is followed for Cu in the n = 4 contiguous chains (pentagons, Fig. 8(a)) and in the n = 5 chains decorated with an extra Cu (hexagons, Fig. 8(a)), although here the chemical potential is not a binding energy, but rather an average energy per Cu atom. These tendencies can be understood by studying the electronic properties of these Cu-graphite systems, e.g., for a Cu absorbed at a step edge, the overlap between 2p states of the edge C atoms and 3d states of the Cu atoms determines the binding strength between C and Cu. An analysis from the density of states (DOS) of electrons for Cu at at zz, ac, and zz57 step edges is provided in Appendix B.

Next, we compare μ_{Cu} values, varying n at a specific type of step edge. For the least-stable zz step, μ_{Cu} increases as n increases from 1 to 4 to 5 (see Figs. 5 and 8(b)). For the most stable zz57 step, the situation is opposite: μ_{Cu} decreases as n increases from 1 to 4 to 5 (see Figs. 7 and 8(b)). These two progressions indicate that the binding of Cu is, on average, reduced by interaction with other Cu atoms at the zz step, but is enhanced by interaction with other Cu atoms at the zz57 step. The ac step is intermediate, both in its stability and in the progression of μ_{Cu}, which increases as n increases from 1 to 4, then decreases from 4 to 5 (see Figs. 6 and 8(b)). This indicates a subtler situation, in which Cu is, on average, initially destabilized by going from a single atom to a chain, then is re-

stabilized when a Cu atom attaches to the chain. For reference, the cohesive energy E_{coh} for bulk Cu is also shown in Fig. 8(b) as a comparison.

Our calculations reveal some interesting subtleties in Cu binding at graphite steps that are worth mentioning. First, from the side views in Figs. 5 to 7, Cu atoms sometimes relax to positions with heights significantly deviating from that of the top GML plane. This is particularly true for Cu at ac and zz57 step edges, indicating complex chemical bonding modes between Cu and C atoms depending on the number of Cu atoms as well as the type of the graphite step edges. Second, there can be significant interactions between Cu atoms at sub-saturated step edges. For instance, Figs. 6(b) and 6(c) again with unit cell width $n_{\mathrm{width}} = 4$ show configurations for $n = 2$ (every second binding site populated) and $n = 3$ (three out of 4 binding sites populated) at the ac step. Both have lower μ_{Cu} than $n = 1$ (at the same adsorption site), with $n = 2$ showing a deep minimum in μ_{Cu}. The Cu atoms for $n = 2$ in Fig. 6(b) are too far apart for a direct Cu-Cu bond, so this indicates a strong indirect attraction between Cu atoms at these second-nearest-neighbor (2NN) positions. On the other hand, Fig. 7(b) shows an $n = 2$ configuration at the zz57 step, and its chemical potential is higher than $n = 1$. At the same time, the Cu atoms have moved away from the most-favored site shown in Fig. 7(a) to form a Cu-Cu bond. This implies that there are strong repulsive interactions between Cu atoms at 2NN favored sites.

IV. ENERGETICS OF Cu DIFFUSION AND INTERCALATION

Here we analyze the energetics relevant to a Cu atom moving from the top graphite terrace, to a step edge (already decorated or not by Cu atoms), to the gallery beneath the top GML. To do this, we shift focus from μ_{Cu} to E_{bind}, since E_{bind} allows evaluation of energetics as a single Cu atom moves between configurations. As discussed in Sec. III, the diamonds in Fig. 8(a) represent the trend in E_{bind} as a function of step stability when $n = 1$ (where $E_{\mathrm{bind}} = \mu_{\mathrm{Cu}}$). The data in Fig. 8(c) show the variation in E_{bind} from $n = 1$ to 5, for each of the three steps. Upon going from n=1 to 5, E_{bind} increases for the zz step, decreases for the zz57 step, and shows intermediate behavior for the ac step. This means that if binding of an isolated Cu atom to a step edge is strong, then decorating the step with a Cu chain makes it much easier to detach an additional Cu atom from the step, and *vice versa*.

The values of E_{bind} are plotted as horizontal lines in the middle of Fig. 9. On the left side (right side) is the E_{bind} value for one Cu atom on top of (beneath the top) GML, previously determined as -0.500 (-1.000) eV [19], using the same DFT method as in this work. The activation barrier, $E_{\mathrm{act}}(\mathrm{s} \rightarrow \mathrm{t})$ or $E_{\mathrm{act}}(\mathrm{s} \rightarrow \mathrm{i})$, for a Cu atom to move from the step edge (s) to the top terrace (t) or to an intercalation site in the gallery (i), respectively, is at a minimum the binding energy difference, $\Delta E_{\mathrm{bind}}(\mathrm{s} \rightarrow \mathrm{t})$ or $\Delta E_{\mathrm{bind}}(\mathrm{s} \rightarrow \mathrm{i})$, between the middle level and the left-hand or right-hand side, respectively, *plus* the relevant diffusion barrier for a Cu atom on the top terrace, E_{dt}, or intercalated in the gallery, E_{di}. The values of the binding energy difference terms are $\Delta E_{\mathrm{bind}}(\mathrm{s} \rightarrow \mathrm{t}) = 1.9$ to 3.6 eV and $\Delta E_{\mathrm{bind}}(\mathrm{s} \rightarrow \mathrm{i}) = 1.4$ to 3.1 eV. For a Cu atom attached to any given step edge configuration, ΔE_{bind} is always 0.5 eV lower for the path into the gallery than to the top of the graphite terrace (see Fig. 9). We will conclude below that $\Delta E_{\mathrm{bind}}(\mathrm{s} \rightarrow \mathrm{i})$ corresponds to the effective barrier for intercalation.

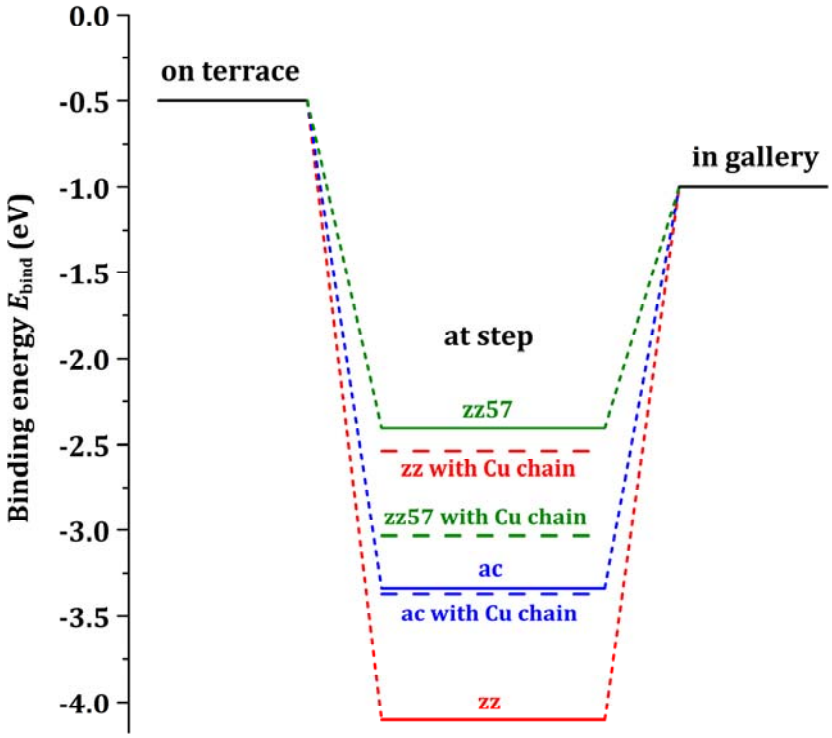

FIG. 9. The binding energy levels of one Cu atom on the graphite terrace, at a step, and in the gallery beneath the top GML. A solid level in the middle denotes the binding energy at a clean graphite step, and a dashed level denotes the binding energy at steps decorated by a Cu chain (corresponding to n = 5 geometries in Figs. 5 to 7). Colors identify the type of a step edge.

We can evaluate the diffusion barriers, E_{dt} and E_{di}, for the top terrace and gallery, respectively, using the climbing nudged elastic band (CNEB) method [40, 41]. The adsorption sites considered are shown in Fig. 10(a). For a Cu atom adsorbed on top of graphite, we have previously reported that the most favorable adsorption site is tTH, where $E_{\mathrm{bind}} = -0.500$ eV [19]. The adsorption energies at other local-equilibrium sites, tTT, tBM, and tHT, are -0.495, -0.494, and -0.337 eV, respectively. Adsorption of a Cu atom at tMB, tCC, and tMM sites is unstable, and the adatom moves to a local minimum close to the initial site after full relaxation. Together, this information indicates that the minimum energy path leading to long-range diffusion of the adsorbed Cu atom is tTH → tBM → tTT → tBM → tTH, for which we obtain $E_{\mathrm{dt}} = 0.008$ eV from CNEB. The energy profile along this minimum energy path (MEP) is shown in Fig. 10(b). On the other hand, for the intercalated Cu atom, the lowest-energy local-equilibrium sites are iCC, iMB, iBM, and iMM, where E_{bind} is -1.000, -1.000, -0.995, and -0.979 eV, respectively. For long-range diffusion in the galleries, the MEP is iCC → iMB → iCC → iMM → iCC→ iBM → iCC. Our CNEB results show that energy barriers to cross between pairs of these sites are simply the differences in the binding energies, i.e. 0.000 eV for iCC → iMB, 0.021 eV for iCC → iMM, and 0.005 eV for iCC → iBM, so the highest barrier (i.e., the global barrier) along the entire MEP is $E_{\mathrm{di}} = 0.021$ eV (see Fig. 10(c)). Compared with ΔE_{bind}, which is in the range from 1.4 to 3.6 eV, the two diffusion barriers $E_{\mathrm{dt}} = 0.008$ eV and $E_{\mathrm{di}} = 0.021$ eV are negligibly small. This means that, to a good approximation, the minimum value of the total activation barrier for a Cu atom to detach from a step is $E_{\mathrm{act}}(\mathrm{min}) \approx \Delta E_{\mathrm{bind}}$.

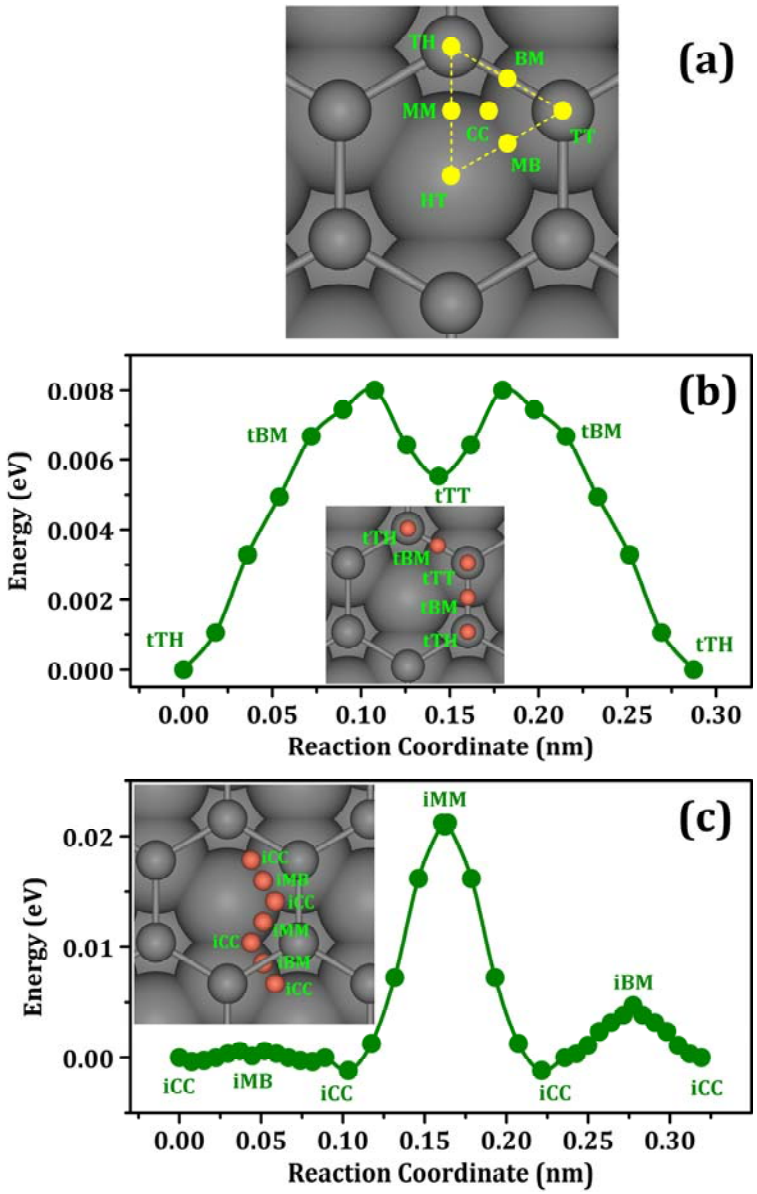

FIG. 10. (a) Schematic representation of different adsorption sites on the basal plane of graphite. Small gray spheres represent the top GML, and larger spheres represent the lower GML. In labeling the sites, the uppercase letters T, H, B, M, and C stand for top, hollow, bridge, midpoint, and center, respectively. The two capital letters denote locations with respect to the first (top) and second (lower) GML, respectively. In addition, a lowercase letter denotes whether the Cu atom is on top (t) or intercalated in the gallery (i). (b) The MEP of a Cu atom (absorbed on top of graphite) diffusing from a tTH site to its nearest-neighbor tHT site. (c) A long-range MEP of a Cu atom (intercalated beneath the top GML) diffusing from an iCC site to other iCC sites. In (b) or (c), the inset schematically shows the sites that the Cu atom crosses along the corresponding MEP. The curves are from our CNEB calculations and generated from a modified Bézier method [42] by fitting the data points versus reaction coordinates. Green dots on a curve represent CNEB images.

For the ac or zz step, there is some evidence that $E_{\rm act}(\rm min)$ estimated from the above $\Delta E_{\rm bind}$ value is close to the real barrier, i.e. there is no additional activation barrier associated with a transition state, such as an Ehrlich-Schwoebel barrier. For these two step configurations, in some calculations we initially positioned a Cu atom at several sites (atop or beneath the top graphene layer) within an appropriately-selected distance from the step edge and allowed the configuration to relax fully. We found that the Cu atom always moved toward the step edge and finally stabilized at an edge position that was not higher than the plane of the top graphene layer. Thus, we speculate that the extra barrier for these two configurations would be zero, and that the behavior may be similar for other types of steps. However, extensive CNEB calculations would be needed to test this conjecture.

In Secs. III and IV, we have only considered 3 types of steps. Other steps with intermediate stability are the ac5666 and ac677 (Fig. 4). Like the ac step, we expect those to show trends and correlations intermediate between zz and zz57 discussed above. Specifically, we expect that the $E_{\rm bind}$ values for a Cu atom at clean ac5666 and ac677 steps should be within the range -4.1 to -2.4 eV, as shown in the middle of Fig. 9.

V. DISCUSSION

It is clear that the minimum barrier, $\Delta E_{\rm bind}(\rm s \rightarrow i)$, for intercalation of a Cu atom bound at the step edge depends sensitively on the configuration of C and Cu atoms at the step. The trends and correlations among different steps, developed throughout Secs. II to IV, lead to the following broad picture. The Cu-C bond strength is clearly determined by the stability of the clean graphite step, being strongest at the least-stable step, the zz step (see Fig. 8(a)). This alone would not be surprising. However, if the Cu-C bond is strong, as in the zz case, then decorating the step with a Cu chain facilitates intercalation, as a Cu atom attached at a fully-decorated step edge is more weakly bonded and thus can more readily detach. Conversely, if the Cu-C bond is weak (e.g., for zz57 step), then formation of a Cu chain impedes intercalation. This nuanced result was unanticipated. Furthermore, the effect is so dramatic that it causes a crossover in $E_{\rm bind}$ and hence $E_{\rm act}(\rm min)$ upon going from a bare graphite step to a Cu-chain-decorated step (see Fig. 8(c) and Fig. 9): Intercalation is easier at zz57 than zz if the step is clean, but harder at zz57 than zz if the step is saturated by a chain. In a simplistic sense, this reflects an oscillatory effect on bonding interaction for Cu in the chain: If Cu interacts strongly with the graphite step, the bond between the Cu chain and extra Cu atom is weakened, and *vice versa*.

The original two issues raised in Sec. I — whether the barrier for Cu intercalation at a step or vacancy depends on C atom arrangement, and whether it depends on Cu decoration — are hence inseparable, since the C atom configuration determines the effect of chain decoration.

Next, we discuss the ramifications of our energetics results for the kinetics of Cu intercalation on graphite. The key observation is that one can realize a relatively low barrier for intercalation of $\Delta E_{\rm bind}(\rm s \rightarrow i) \approx 1.4$ to 1.5 eV for either stable undecorated zz steps or unstable fully Cu-decorated zz57 steps. This corresponds to a detachment rate of

$h_{\mathrm{detach}} \approx 10^4$/s for an attempt frequency of ~10^{13}/s. If one estimates the density of active portals to be around 10^2/μm^2. Then, the "capture zone" area per portal is around 10^4 nm^2, and the rate of arrival of atoms at the portal (in the absence of surface island formation) is somewhat above $h_{\mathrm{arrive}} \approx 10^3$/s for a typical deposition flux of 0.01 monolayers/s. Thus, since $h_{\mathrm{detach}} > h_{\mathrm{arrive}}$, detachment is sufficiently facile to avoid accumulation of atoms at the portal thereby enabling intercalation. One the other hand, for higher intercalation barriers of 2 eV or above, $h_{\mathrm{arrive}} > h_{\mathrm{detach}}$, and then the portals are expected to become blocked due to accumulating metal atoms at the portal.

We can speculate on how these results pertain to intercalation at vacancies. The most reactive (least-stable) step is the zz, which has cus-C atoms locked into nearly 120° vertices at the step edge. Some vacancies, such as those shown in Figs. 2(a), 2(c), 2(e), and 2(f) have similar cus-C atoms, so they may behave like a zz step. That is to say, they present a high barrier to intercalation when clean, and tend to become blocked by adsorbed Cu atoms. We thus expect these vacancies to be inactive for intercalation unless they are very large. Other vacancies have no cus-C atoms, as in Figs. 2(b) and 2(d) due to reconstruction. We expect these vacancies to be similar to a very stable step edge, presenting a low barrier to intercalation even when clean. We can speculate that these types of vacancies are the active portals detected in experiments.

VI. CONCLUSIONS

To elucidate the energetics of Cu intercalation in graphite, we have calculated the chemical potentials and binding energies for Cu in three main configurations at graphite step edges: an isolated atom, a contiguous chain, and an atom attached to a chain. For Cu interacting directly with a graphite step edge, the strength of the interaction depends on the stability of the step, with Cu interacting more strongly at the less-stable step. However, the relationship is reversed when considering binding of the Cu atom attached to a step edge saturated by a Cu chain. Taken together, these trends mean that if the graphite step is less stable, as in the zz case, then decorating the step with a Cu chain facilitates intercalation, and *vice versa*.

This analysis requires the step energies for graphite steps. We have calculated zz, ac677, ac5666, ac, and zz57 geometries and compared with similar behavior for GML steps. A given configuration is always more stable on graphite; furthermore, the near-degeneracy that exists between zz57 and ac in graphene is lifted in graphite. A new edge geometry, ac5666, is found to be moderately stable in both graphite and graphene.

In principle, the diffusion barriers for atomic Cu on top of a graphite terrace, and within the uppermost graphite gallery, contribute to the total barrier for a Cu atom to detach from the step edge. This is true regardless of whether its final state is on top of a terrace or in a gallery (intercalated). The diffusion barriers are $E_{\mathrm{dt}} = 0.008$ eV (on top) and $E_{\mathrm{di}} = 0.021$ eV (in gallery). These barrier values are negligibly small relative to the binding energy differences between a step and terrace, or between a step and gallery. This leads to the

conclusion that the minimum barrier for intercalation (starting from a step) is 1.4 to 3.1 eV, depending on the configuration at the step. Similarly, the minimum barrier for moving from a step to a terrace is 1.9 to 3.6 eV. For a Cu atom attached to any given step edge configuration, this minimum barrier is always 0.5 eV lower for the path into the gallery than to the top of the graphite terrace. There is some indication that an extra activation barrier to step detachment, such as an Ehrlich-Schwoebel barrier, is small or zero, at least at the clean graphite step.

Acknowledgements

This work was supported mainly by the U. S. Department of Energy (DOE), Office of Science, Basic Energy Sciences, Materials Sciences and Engineering Division. Research was performed at the Ames Laboratory, which is operated by Iowa State University under contract No. DE-AC02-07CH11358. DFT calculations were performed, in part, with a grant of computer time at the National Energy Research Scientific Computing Centre (NERSC). NERSC is a DOE Office of Science User Facility supported by the Office of Science of the U.S. DOE under Contract No. DE-AC02-05CH11231. The calculations also used the Extreme Science and Engineering Discovery Environment (XSEDE), which is supported by National Science Foundation under Grant No. ACI-1548562. The participation of J.W.E was supported by the U. S. DOE, Office of Science, Basic Energy Sciences, Chemical Sciences, Geosciences, and Biosciences Division.

APPENDIX A: BENCHMARKING AND ADDITIONAL DETAILS OF DFT ANALYSIS

We first benchmark the bulk properties (lattice constants and cohesive energies) of graphite, graphene, and Cu. For graphite, we use the conventional unit cell in which 4 atoms are included and the hexagonal structure is AB-stacked [43]. For a graphene monolayer (GML), or face-centered cubic (fcc) Cu bulk, we use the corresponding primitive unit cell in which only one atom is contained. Table II lists the lattice constants and cohesive energies of hexagonal graphite, graphene, and fcc Cu from this work and previous experiments. From Table II, the optB88-vdW functional reproduces well experimental lattice constants and cohesive energies of graphite, graphene, and Cu. The cohesive energy is calculated as $E_{\mathrm{coh}} = E_{\mathrm{gas}} - \sigma_{\mathrm{bulk}}$, where σ_{bulk} is the energy per atom in the unit cell, and E_{gas} is the energy of one atom in gas phase.

Table II. Lattice constants (a and c, or a) and cohesive energies (E_{coh}) of hexagonal graphite, graphene, and fcc Cu from our DFT calculations versus previous experiments. The $\boldsymbol{k}$ meshes and cutoff energies (E_{cut}) used in our DFT calculations are also listed.

System	Method	E_{cut} (eV)	$\boldsymbol{k}$ mesh	a (nm)	c (nm)	E_{coh} (eV)
graphite	optB88-vdW	1000	$41 \times 41 \times 41$	0.2465	0.6701	7.800
	experiment			0.24589[a]	0.66720[b]	7.37[c]
graphene	optB88-vdW	1000	$41 \times 41 \times 41$	0.2464		7.730
	experiment			0.24[d]		
Cu	optB88-vdW	600	$51 \times 51 \times 51$	0.3629		3.580
	experiment			0.36024[e]		3.49[c]

[a]At 78 to 298 K [44].
[b]At 4.2 K [44].
[c]Ref. [45].
[d]Ref. [46].
[e]Extrapolated to 0 K [47].

Using a DFT-based tight-binding (DFTB) method, Kotakoski *et al*. calculated the vacancy formation energies E_{vf} for different numbers of missing C atoms in freestanding graphene [28]. Here we use the optB88-vdW functional to calculate the E_{vf} values corresponding to the fully-relaxed structures for m = 1 to 6 in Fig. 2, where the arrangement of C atoms for a given m is of the largest central hole (which is of most interest for intercalation studies). The E_{vf} values for m = 1, 2, and 3 from our optB88-vdW calculations are in reasonable agreement with those obtained by Kotakoski *et al*. [29], as well as those from Ronchi *et al*. using a hybrid functional of B3LYP-D* and Grimme's PBE-D2 functional for m = 1 [30], as listed in Table III.

Table III. Graphene vacancy formation energies E_{vf} (in eV) of 6 defective structures with the largest central holes for m = 1 to 6 corresponding to those in Fig. 2. The vacancy formation energy is calculated from $E_{vf} = E_{df} - N_C\sigma_{GML}$, where E_{df} is the total energy of the defective graphene with m missing C atoms, N_C is the total number of C atoms in the defective graphene, and σ_{GML} is the energy per C atom in a freestanding perfect GML without any defects. In these calculations for different m, we always use a rectangular supercell size of $8 \times 4\sqrt{3}$ (in units of $a_C = 0.2465$ nm) with the $\boldsymbol{k}$ mesh of $5 \times 5 \times 1$.

m	optB88-vdW	DFTB	B3LYP-D*	PBE-D2
1	7.66	7.38[a]	8.05 to 8.18[b]	7.53 to 7.90[c]
2	7.68	7.52[a]		
3	10.92	10.67[a]		
4	11.22			
5	15.04			
6	17.50			

[a]Ref. [28].
[b]Obtained from different supercells [32].
[c]Obtained from different supercells and simulation packages [32].

With regard to analysis of step energies as described in Sec. II, according to previous calculations [36, 48], the value of ε_{edge} is not sensitive to the ribbon width w if w is sufficiently large. On this basis, we choose w for 5 types of edges, as listed in Table IV. In the calculations for any specific GML edge and its corresponding graphite step edge, we use the identical supercell size, GML ribbon width w, and $\boldsymbol{k}$ mesh (see Table IV).

Table IV. Supercell sizes, GML ribbon widths, and $\boldsymbol{k}$ meshes used in our DFT calculations for 5 types of GML edges or graphite step edges. All lengths are in units of lattice constant a (listed in Table III) of GML or graphite.

Edge or step type	Supercell size	GML ribbon width w	$\boldsymbol{k}$ mesh
zz	$4 \times 3\sqrt{3}$	$3\sqrt{3}/2$	$11 \times 7 \times 1$
ac677	$2\sqrt{3} \times 8$	5	$11 \times 7 \times 1$
ac5666	$2\sqrt{3} \times 8$	4	$11 \times 7 \times 1$
ac	$2\sqrt{3} \times 6$	3	$11 \times 7 \times 1$
zz57	$2 \times 6\sqrt{3}$	$4\sqrt{3}$	$19 \times 3 \times 1$

APPENDIX B: DOS ANALYSIS FOR Cu AT GRAPHITE EDGES

To understand why the order of the Cu binding (or adsorption) strengths is opposite to the order of the stabilities of 3 types of clean step edges in Sec. III, using the optB88-vdW functional we calculate and plot the projected density of states (PDOS) of a Cu atom adsorbed at zz, ac, and zz57 edge and its NN edge C atom in Figs. 11(a), 11(b), and 11(c), the geometries of which correspond to Figs. 5(a), 6(b), and 7(a), respectively. It is obvious

that, in contrast to Figs. 11(b) and 11(c), Fig. 11(a) has much larger PDOS magnitudes below and near the Fermi level, and particularly much larger overlap of 2p states of the edge C atom and 3d states of the Cu atom. As shown in Fig. 11, the overlap between 2p and 3d states is mainly from the contribution of $2p_y$ states (red-colored line) of the edge C atom and $3d_{xy}$, $3d_{yz}$, $3d_{z^2}$, or $3d_{x^2-y^2}$ states of the Cu atom. The larger overlap corresponds to stronger binding between the edge C and Cu atoms. Below and near the Fermi level, the overlap especially between $2p_y$ and $3d_{xy}$ states becomes much smaller from Fig. 11(a) to Fig. 11(b) and then to Fig. 11(c). This therefore explains the order of the C-Cu binding strengths from stronger to weaker for Cu at zz to ac to zz57 edge, as indicated by the curve with diamonds in Fig. 8(a).

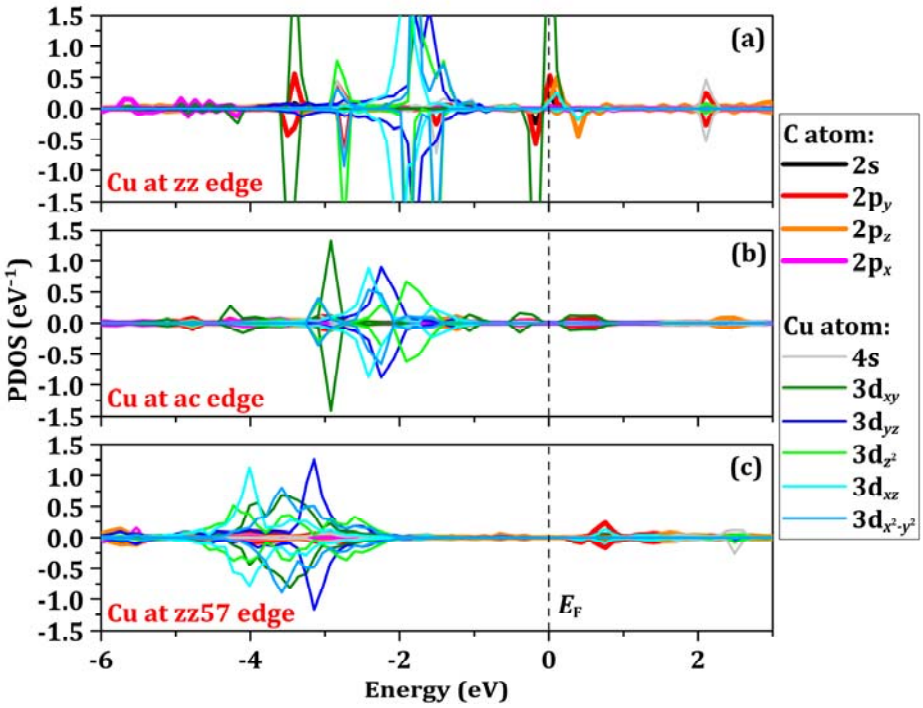

FIG. 11. (a) PDOS of the Cu atom adsorbed at a zz edge and its NN edge C atom in the configuration of Fig. 5(a). (b) PDOS of a Cu atom adsorbed at an ac edge and its NN edge C atom in the configuration of Fig. 6(b). (c) PDOS of the Cu atom adsorbed at a zz57 edge and its NN edge C atom in the configuration of Fig. 7(a). The positive (negative) PDOS represents the spin-up (spin-down) states. The *x* and *y* axis in (a), (b), or (c) are always along the directions parallel and vertical to the edge, respectively, while the *z* axis is always perpendicular to the surface terrace and upward. The energy zero is always set to be the Fermi level E_F. The warm-colored lines indicate three 2p states of the edge C atom, and the cold-colored lines indicate five 3d states of the Cu atom, as indicated by the legend. The black- and gray lines indicate 2s and 4s states of the edge C and Cu atom, respectively.

References:

[1] M. S. Dresselhaus and G. Dresselhaus, Adv. Phys. **51**, 1 (2002).

[2] G. Li, Y.-Y. Zhang, H. Guo, L. Huang, H. Lu, X. Lin, Y.-L. Wang, S. Du, and H.-J. Gao, Chem. Soc. Rev. **47**, 6073 (2018).

[3] Z. Lin, Y. Lei, S. Subramanian, N. Briggs, Y. Wang, C.-L. Lo, E. Yalon, D. Lloyd, S. Wu, K. Koski, R. Clark, S. Das, R. M. Wallace, T. Kuech, J. S. Bunch, X. Li, Z. Chen, E. Pop, V. H. Crespi, J. A. Robinson, and M. Terrones, APL Mater. **6**, 080701 (2018).

[4] P. Solís-Fernández, M. Bissett, and H. Ago, Chem. Soc. Rev. **46**, 4572 (2017).

[5] J. Wan, S. D. Lacey, J. Dai, W. Bao, M. S. Fuhrer, and L. Hu, Chem. Soc. Rev. **45**, 6742 (2016).

[6] X. Liu, Y. Han, J. W. Evans, A. K. Engstfeld, R. J. Behm, M. C. Tringides, M. Hupalo, H.-Q. Lin, L. Huang, K.-M. Ho, D. Appy, P. A. Thiel, and C.-Z. Wang, Prog. Surf. Sci. **90**, 397 (2015).

[7] M. Batzill, Surf. Sci. Rep. **67**, 83 (2012).

[8] L. Yang, F. Zhao, Y. Zhao, Y. Sun, G. Yang, L. Tong, and J. Zhang, Carbon **138**, 390 (2018).

[9] A. Ambrosi and M. Pumera, Chem. Soc. Rev. **47**, 7213 (2018).

[10] K. Shen, H. Sun, J. Hu, J. Hu, Z. Liang, H. Li, Z. Zhu, Y. Huang, L. Kong, Y. Wang, Z. Jiang, H. Huang, J. W. Wells, and F. Song, J. Phys. Chem. C **122**, 21484 (2018).

[11] F. Jiang, Y. Yu, Y. Wang, A. Feng, and L. Song, Mater. Lett. **200**, 39 (2017).

[12] N. I. Kovtyukhova, N. Perea-López, M. Terrones, and T. E. Mallouk, ACS Nano **11**, 6746 (2017).

[13] A. M. Abdelkader, A. J. Cooper, R. A. W. Dryfe, and I. A. Kinloch, Nanoscale **7**, 6944 (2015).

[14] P. Leicht, L. Zielke, S. Bouvron, R. Moroni, E. Voloshina, L. Hammerschmidt, Y. S. Dedkov, and M. Fonin, ACS Nano **8**, 3735 (2014).

[15] M. Sicot, P. Leicht, A. Zusan, S. Bouvron, O. Zander, M. Weser, Y. S. Dedkov, K. Horn, and M. Fonin, ACS Nano **6**, 151 (2012).

[16] T. P. Kaloni , M. U. Kahaly , Y. C. Cheng, and U. Schwingenschlögl, J. Mater. Chem. **22**, 23340 (2012).

[17] Y. Zhang, Y. Zhang, D. Ma, Q. Ji, W. Fang, J. Shi, T. Gao, M. Liu, Y. Gao, Y. Chen, L. Xu, and Z. Liu, Nano Res. **6**, 887 (2013).

[18] A. Lii-Rosales, Y. Han, K. M. Yu, D. Jing, N. Anderson, D. Vaknin, M. C. Tringides,

J. W. Evans, M. S. Altman, and P. A. Thiel, Nanotechnology **29**, 505601 (2018).

[19] A. Lii-Rosales, Y. Han, J. W. Evans, D. Jing, Y. Zhou, M. C. Tringides, M. Kim, C.-Z. Wang, and P. A. Thiel, J. Phys. Chem. C **122**, 4454 (2018).

[20] Y. Zhou, A. Lii-Rosales, M. Kim, M. Wallingford, D. Jing, M. C. Tringides, C.-Z. Wang, and P. A. Thiel, Carbon **127**, 305 (2018).

[21] Y. Han, A. Lii-Rosales, Y. Zhou, C.-J. Wang, M. Kim, M. C. Tringides, C.-Z. Wang, P. A. Thiel, and J. W. Evans. Phys. Rev. Mater. **1**, 053403 (2017).

[22] C. Subramaniam, T. Yamada, K. Kobashi, A. Sekiguchi, D. N. Futaba, M. Yumura, and K. Hata, Nat. Commun. **4**, 2202 (2013).

[23] O. Lehtinen, J. Kotakoski, A. V. Krasheninnikov, A. Tolvanen, K. Nordlund, and J. Keinonen, Phys. Rev. B **81**, 153401 (2010).

[24] S. Habenicht, W. Bolse, H. Feldermann, U. Geyer, H. Hofsäss, K. P. Lieb, and F. Roccaforte, Europhys. Lett. **50**, 209 (2000).

[25] M. Büttner, P. Choudhury, J. K. Johnson, and J. T. Yates Jr., Carbon **49**, 3937 (2011).

[26] L. Yu, C. Du, and X. Liu, Mater. Res. Express **5**, 025022 (2018).

[27] G.-D. Lee, C. Z. Wang, E. Yoon, N.-M. Hwang, D.-Y. Kim, and K. M. Ho, Phys. Rev. Lett. **95**, 205501 (2005).

[28] J. Kotakoski, A. V. Krasheninnikov, and K. Nordlund, Phys. Rev. B **74**, 245420 (2006).

[29] F. Banhart, J. Kotakoski, and A. V. Krasheninnikov, ACS Nano **5**, 26 (2011).

[30] J. C. Meyer, C. Kisielowski, R. Erni, M. D. Rossell, M. F. Crommie, and A. Zettl, Nano Lett. **8**, 3582 (2008).

[31] J. Kotakoski, A. V. Krasheninnikov, U. Kaiser, and J. C. Meyer, Phys. Rev. Lett. **106**, 105505 (2011).

[32] C. Ronchi, M. Datteo, D. Perilli, L. Ferrighi, G. Fazio, D. Selli, and C. D. Valentin, J. Phys. Chem. C **121**, 8653 (2017).

[33] G. Kresse and J. Furthmüller, Phys. Rev. B **54**, (1996) 11169.

[34] G. Kresse and D. Joubert, Phys. Rev. B **59**, 1758 (1999).

[35] J. Klimeš, D. R. Bowler, and A. Michaelides, J. Phys.: Cond. Matt. **22**, 022201 (2010).

[36] P. Koskinen, S. Malola, and Hannu Häkkinen, Phys. Rev. Lett. **101**, 115502 (2008).

[37] P. Koskinen, S. Malola, and Hannu Häkkinen, Phys. Rev. B **80**, 073401 (2009).

[38] Ç. Ö. Girit, J. C. Meyer, R. Erni, M. D. Rossell, C. Kisielowski, L. Yang, C.-H. Park, M. F. Crommie, M. L. Cohen, S. G. Louie, and A. Zettl, Science **323**, 1705 (2009).

[39] Y. Niimi, T. Matsui, H. Kambara, K. Tagami, M. Tsukada, and H. Fukuyama, Phys. Rev. B **73**, 085421 (2006).

[40] G. Henkelman, B. P. Uberuaga, and H. Jónsson, J. Chem. Phys. **113**, 9901 (2000).

[41] G. Henkelman and H. Jónsson, J. Chem. Phys. **113**, 9978 (2000).

[42] G. Farin, *Curves and Surfaces for CAGD: A Practical Guide*, 5th ed. (Academic, San Diego, 2002).

[43] J. D. Bernal, Proc. R. Soc. A **106**, 749 (1924).

[44] V. Baskin and L. Meyer, Phys. Rev. **100**, 554 (1955).

[45] C. Kittel, *Introduction to Solid State Physics*, 7th ed. (John Wiley & Sons, New York, 1996).

[46] M. H. Gass, U. Bangert, A. L. Bleloch, P. Wang, R. R. Nair, and A. K. Geim, Nat. Nanotechnol. **3**, 676 (2008).

[47] A. K. Giri and G. B. Mitra, J. Phys. D **18**, L75 (1985).

[48] B. Huang, M. Liu, N. Su, J. Wu, W. Duan, B. Gu, and F. Liu, Phys. Rev. Lett. **102**, 166404 (2009).